Experimental Evaluation of Haptic Control for Human Activated Command Devices

Andrew Zammit Mangion * **Simon G. Fabri** **

Faculty of Engineering, University of Malta, Msida, MSD 2080, Malta
* *Tel: +356 (7906)1312; e-mail: andrewzm@ieee.org*
** *Tel: +356 (2340)2079; e-mail: sgfabr@eng.um.edu.mt*

Abstract: Haptics refers to a widespread area of research that focuses on the interaction between humans and machine interfaces as applied to the sense of touch. A haptic interface is designed to increase the realism of tactile and kinesthetic sensations in applications such as virtual reality, teleoperation, and other scenarios where situational awareness is considered important, if not vital. This paper investigates the use of electric actuators and non-linear algorithms to provide force feedback to an input command device for providing haptics to the human operator. In particular, this work involves the study and implementation of a special case of feedback linearization known as inverse dynamics control and several outer loop impedance control topologies. It also investigates the issues concerned with force sensing and the application of model based controller functions in order to vary the desired inertia and the desired mass matrix. Results of the controllers' abilities to display any desired impedance and provide the required kinesthetic constraint of virtual environments are shown on two experimental test rigs designed for this purpose.

Keywords: Haptics, Impedance control, Force feedback, Haptic rendering, Virtual objects

1. INTRODUCTION

Research in haptics focuses on the physical interaction between humans and machine interfaces. A haptic interface is designed to increase the realism of tactile and kinesthetic sensations in applications such as virtual reality, teleoperation, and other scenarios where situational awareness is considered important and where visual stimulation alone is considered insufficient for conveying the full realism of the situation (which could be real or virtual) with which the human is interacting. Haptic interfaces which convey kinesthetic information through the use of force feedback devices have been applied in several applications such as simulators for surgeon training, pilot training, computer-aided design (CAD), graphic arts, computer games and others (Stone [2000], Hayward et al. [2004]).

The performance of the haptic interface device can be evaluated according to the achievable precision in displaying a desired mechanical impedance (Carignan and Clear [2000]). One of the haptic controller's aims is to cancel out the interface device's natural dynamics such that they are not perceived by the human operator as part of the simulated environment. Inherent system anomalies such as static friction, backlash and sensor quantization, diminish the quality of the haptic experience and should be kept to a minimum.

Impedance and admittance control schemes have been investigated in detail and applied to several robotic manipulators differing in structure and application. The well known PHANTOM range of haptic interfaces are hand-held desktop devices driven by DC motors combined with a cable transmission system to a linkage for backlash reduction (Massie and Salisbury Jr. [2002]) and make use of an impedance control topology (Carignan and Clear [2000]). On the other hand the FCS Control Systems HapticMaster employs an admittance control topology and is capable of displaying forces an order of magnitude larger than the PHANTOM (Massie and Salisbury [1994], Linde et al. [2002]). The 3 degrees-of-freedom (DOF) Spherical Haptic Device (SHaDe) at the University of Laval (Birglen et al. [2002]) and the 3 DOF Cartesian manipulator Excalibur at the University of Washington, Seattle (Adams [1999]) are just two of several other devices built for haptic exploration.

Despite ongoing research and various publications on haptics, there is a lack of papers which provide a complete overview of the development of a haptic system starting from the mechanical design stages through to controller implementation together with experimental results. The aim of this paper is to address this gap by presenting a framework for the design of haptic controlled devices from a practical, systems engineering standpoint. This is achieved by providing full implementation details of a complete integrated haptic controller; from inner loop control through to inverse dynamics control and outer loop impedance control. A series of control laws, some incorporating force sensing and others not, are considered. The application of model based controller functions in order to vary the desired inertia and the desired mass matrix is also demonstrated. Results of the controllers' abilities to display any desired impedance and provide the required kinesthetic constraint of virtual environments are shown

on two different test rigs designed for effecting haptic display in one and two dimensions respectively.

Section 2 of the paper describes the underlying control methodology. Section 3 presents the details of different impedance controller configurations, whilst the approach used to create virtual objects is described in Section 4. Section 5 describes the experiment setup and results are presented and evaluated in Section 6. Finally, Section 7 concludes the paper.

2. THE CONTROL METHODOLOGY

The design approach taken in this paper follows an impedance control methodology (Hogan [1985]). It also employs an inverse dynamics controller for effecting feedback linearization so as to cancel out the nonlinear dynamics of the haptic device. In this manner, the impedance control law is then designed on a linear and decoupled plant model so that a closed loop desired impedance is displayed. The complete control architecture is depicted in Fig. 1.

The torque of the motors driving the haptic interface device is controlled according to the values commanded by the impedance and the inverse dynamics control laws through a fast inner-loop current controller implemented on a digital control board. This current controller was designed using discrete-time pole placement techniques with integral action on the digital equivalent of the electrical transfer function of the motor

$$V(s) = I(s)[sL + R]$$

where V, I, L and R represent the armature voltage, current, inductance and resistance respectively. The inner loop sampling rate was set to 7.5kHz and the current controller was configured to give a slightly overdamped response with a closed loop bandwidth of 700Hz. The controller design also takes into account the lag introduced by the anti-aliasing Bessel filters.

The feedback linearization control law was developed next. The haptic interface is a mechanical device whose dynamics are characterized by mathematical equations having a similar form to those of robotic manipulators. Physical links are connected together at joints in some geometrical fashion. The angular displacement of the links at the joints are called joint variables, represented by vector $\mathbf{q}$. The joints, though not necessarily all of them, are actuated by devices that can generate torque. These control torques are represented by a joint torque vector $\mathbf{u}$. Hence, the dynamic equation of the haptic device in joint space is given by (Sciavicco and Siciliano [2000])

$$\mathbf{D}\ddot{\mathbf{q}} + \mathbf{C}\dot{\mathbf{q}} + \mathbf{B}\dot{\mathbf{q}} + \mathbf{g} + \mathbf{J}^{\mathbf{T}}\mathbf{f_l} = \mathbf{u} \tag{1}$$

where $\mathbf{D}$ is the device natural inertia matrix, $\mathbf{C}$ is the matrix containing the centrifugal and Coriolis terms, $\mathbf{B}$ is the viscous damping matrix, $\mathbf{g}$ is the gravity potential vector, $\mathbf{J}$ denotes the system Jacobian and $\mathbf{f_l}$ is the vector of forces applied by the human operator at the end effector where the operator interacts with the device. The position coordinates of the end effector, denoted by vector $\mathbf{x}$ in Cartesian space, are related to the joint variables $\mathbf{q}$ by the forward kinematic equations. The Jacobian $\mathbf{J}$ relates the

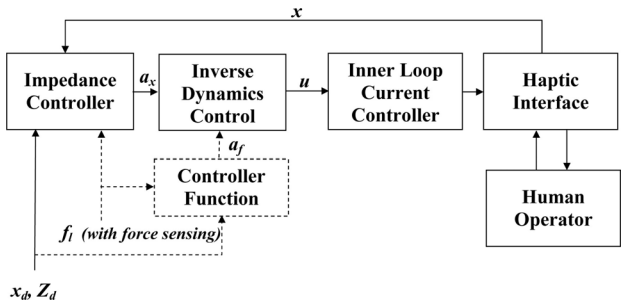

Fig. 1. Haptic controller architecture.

velocities of these variables by the equation $\dot{\mathbf{x}} = \mathbf{J}\dot{\mathbf{q}}$, which leads to

$$\ddot{\mathbf{x}} = \mathbf{J}\ddot{\mathbf{q}} + \dot{\mathbf{J}}\dot{\mathbf{q}}. \tag{2}$$

If one defines an input control torque (Sciavicco and Siciliano [2000])

$$\mathbf{u} = \mathbf{D}\mathbf{a_q} + \mathbf{C}\dot{\mathbf{q}} + \mathbf{B}\dot{\mathbf{q}} + \mathbf{g} + \mathbf{J}^{\mathbf{T}}\mathbf{a_f} \tag{3}$$

where $\mathbf{a_q}$ and $\mathbf{a_f}$ are controller functions that will be suitably formulated later, the system non-linearities can be cancelled out. As a result of the manipulator configuration, the Jacobian $\mathbf{J}$ is a square 2×2 matrix. Therefore, in this case, the inverse Jacobian can be found. Substituting (3) in (1), multiplying by $\mathbf{JD^{-1}}$ and setting

$$\mathbf{a_q} = \mathbf{J}^{-1}(\mathbf{a_x} - \dot{\mathbf{J}}\dot{\mathbf{q}}), \tag{4}$$

where $\mathbf{a_x}$ will be defined later, then it follows from (2) that

$$\ddot{\mathbf{x}} = \mathbf{a_x} - \mathbf{W}(\mathbf{f_l} - \mathbf{a_f}) \tag{5}$$

where $\mathbf{W} = \mathbf{JD^{-1}J^T}$ is the mobility tensor which relates the acceleration of the end point coordinates to the applied force (Hogan [1985]).

Assuming no modeling mismatch, the system is now in linear form and correct manipulation of controller functions $\mathbf{a_x}$ and $\mathbf{a_f}$ can ensure a completely decoupled and linear system to which any desired impedance control law can be applied. The next section will present three ways in which the impedance controller may be configured.

3. IMPEDANCE CONTROLLER CONFIGURATION

The desired impedance that needs to be felt at the haptic interface is specified in terms of a second order linear dynamic equation typical of a mass-spring-damper system. These dynamics are characterized by 3 parameter values that determine the desired stiffness $\mathbf{K_d}$, desired damping $\mathbf{B_d}$ and desired mass (or inertia if rotary) $\mathbf{M_d}$ such that the resultant closed loop equation takes the following form (Spong et al. [2005], Albu-Schäffer and Hirzinger [2002])

$$\mathbf{M_d}\ddot{\tilde{\mathbf{x}}} + \mathbf{B_d}\dot{\tilde{\mathbf{x}}} + \mathbf{K_d}\tilde{\mathbf{x}} = -\mathbf{f_l} \tag{6}$$

where $\tilde{\mathbf{x}} = \mathbf{x} - \mathbf{x_d}$, $\mathbf{x_d}$ being a user-specified reference position in Cartesian space. For simplicity it is assumed that the impedance parameters $\mathbf{K_d}$, $\mathbf{B_d}$ and $\mathbf{M_d}$ are diagonal matrices. The ability to model the haptic device as a desired impedance in the above form constitutes the first step in the process of rendering virtual objects to exhibit any desired apparent mechanical properties. This is

achieved by suitable selection of controller functions $\mathbf{a_q}$, $\mathbf{a_f}$ and $\mathbf{a_x}$. Three possibilities for this are presented next.

3.1 Controller 1 - use of force/torque sensing

The first approach to be considered here is a second order impedance control technique involving the use of sensors for measurement of the force signal $\mathbf{f_l}$. Setting $\mathbf{a_q}$ according to (4), $\mathbf{a_f}$ equal to $\mathbf{f_l}$ and, as shown by Spong et al. [2005], choosing

$$\mathbf{a_x} = \ddot{\mathbf{x}}_\mathbf{d} - \mathbf{M_d^{-1}}(\mathbf{B_d}\dot{\tilde{\mathbf{x}}} + \mathbf{K_d}\tilde{\mathbf{x}} + \mathbf{f_l}), \tag{7}$$

then it follows from (5) that the desired closed loop impedance in (6) is perfectly satisfied. In practice, $\ddot{\mathbf{x}}_\mathbf{d}$ is taken to be zero but is still included for no loss in generality. This controller topology is derived from conventional force-based impedance control techniques such as that shown by Volpe [1990]. Although this approach provides a direct reduction in control law complexity, force sensors can be expensive and inconvenient to implement, depending on the geometry of the haptic interface.

3.2 Controller 2 - no force/torque sensing

Another impedance controller configuration that avoids the use of force sensing but still leads to perfect matching of the desired impedance (6), works by manipulating the function $\mathbf{a_f}$ to cater for the applied force. As in Controller 1, function $\mathbf{a_q}$ is set according to (4) and $\mathbf{a_x}$ as

$$\mathbf{a_x} = \ddot{\mathbf{x}}_\mathbf{d} - \mathbf{M_d^{-1}}(\mathbf{B_d}\dot{\tilde{\mathbf{x}}} + \mathbf{K_d}\tilde{\mathbf{x}}). \tag{8}$$

Substituting (8) into (5) leads to the following expression

$$\mathbf{W^{-1}}(\ddot{\tilde{\mathbf{x}}} + \mathbf{M_d^{-1}B_d}\dot{\tilde{\mathbf{x}}} + \mathbf{M_d^{-1}K_d}\tilde{\mathbf{x}}) - \mathbf{a_f} = -\mathbf{f_l}. \tag{9}$$

Hence, to obtain the desired impedance of (6), it follows that $\mathbf{a_f}$ must be set to:

$$\begin{aligned}\mathbf{a_f} = (\mathbf{W^{-1}} - \mathbf{M_d})\ddot{\tilde{\mathbf{x}}} + (\mathbf{W^{-1}M_d^{-1}B_d} - \mathbf{B_d})\dot{\tilde{\mathbf{x}}} \\ +(\mathbf{W^{-1}M_d^{-1}K_d} - \mathbf{K_d})\tilde{\mathbf{x}}.\end{aligned} \tag{10}$$

In this paper, as a simplification to (10), it is suggested to set the desired mass coefficient of $\ddot{\tilde{\mathbf{x}}}$ in (6) to be equal to the inverse of the mobility tensor $\mathbf{W}$, if this is acceptable to the application at hand. This implies that $\mathbf{a_f} = \mathbf{0}$ in (10). Substituting (8) in (5) then leads to a resultant closed loop impedance

$$\mathbf{W^{-1}}\ddot{\tilde{\mathbf{x}}} + \mathbf{B_d}\dot{\tilde{\mathbf{x}}} + \mathbf{K_d}\tilde{\mathbf{x}} = -\mathbf{f_l}. \tag{11}$$

In this case, the effective displayed mass is totally dependent on the inertia of the haptic device via $\mathbf{W^{-1}}$, which is also, in general, time-varying. If this term is kept very small in magnitude through having a large mobility tensor (*i.e.* a low device inertia), the resultant closed loop impedance will closely approach a first order impedance exhibiting one dominant pole. These two variants of Controller 2 shall be denoted as the first and second variant respectively.

3.3 Controller 3 - no force/torque sensing, no Jacobian inverse or derivative

A controller having similar performance to Controller 2 and which, to the authors' knowledge, has not been previously published, can be obtained by taking advantage of the relationship between the function in Cartesian space $\mathbf{a_f}$ to the linearizing function in joint space $\mathbf{a_q}$. In this case, if instead of using (4) we set $\mathbf{a_q}$ equal to the null vector and let

$$\mathbf{a_f} = -\mathbf{B_d}\dot{\tilde{\mathbf{x}}} - \mathbf{K_d}\tilde{\mathbf{x}}, \tag{12}$$

it follows from (1) and (3) that the resultant closed loop impedance becomes

$$\mathbf{J^{T^{-1}}D}\ddot{\mathbf{q}} + \mathbf{B_d}\dot{\tilde{\mathbf{x}}} + \mathbf{K_d}\tilde{\mathbf{x}} = -\mathbf{f_l} \tag{13}$$

where $\mathbf{J^{T^{-1}}D}\ddot{\mathbf{q}}$ represents the inertial disturbance of the device in Cartesian space and which, like $\mathbf{W^{-1}}$ in (11), is not constant. The advantage of this controller is that $\mathbf{J^{T^{-1}}}$ is now only implicitly evident in the resultant closed loop impedance, whereas before $\mathbf{J^{-1}}$ appeared explicitly in the expression for $\mathbf{a_q}$ (4), resulting in spuriously large control inputs $\mathbf{u}$ in regions where the Jacobian approaches a singularity (for instance at the workspace boundaries). Whilst Controller 2 approaches instability in these regions, at most a relatively larger inertia is felt at these workspace boundaries when using Controller 3. Moreover, the Jacobian derivative is not used in the controller, rendering this control method more resistant to quantization effects.

4. VIRTUAL OBJECTS

The process of virtual object generation is known as haptic rendering. In this paper haptic interaction is assumed to be *point-based* in the sense that only a single point representing the manual probe is assumed to exist in virtual space.

Adopting the notion depicted in McLaughlin et al. [2002], the mechanical constraint of a virtual object can be simulated by applying the above control laws to an impedance modeled between the so-called *manual proxy* and its virtual counterpart as shown in Fig. 2. These two points can also be referred to as the Haptic Interface Point (HIP) and the Ideal Haptic Interface Point (IHIP) respectively. If the two proxies are configured to collocate (track each other), then free space is simulated. Fixing the virtual proxy in space would generate an impedance in accordance with the desired parameters $\mathbf{K_d}$, $\mathbf{B_d}$ and $\mathbf{M_d}$ as the HIP

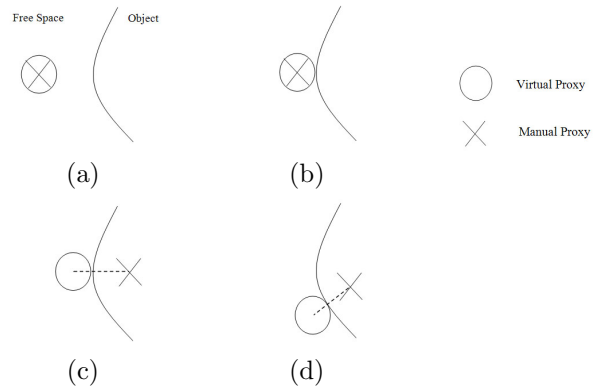

Fig. 2. (a) Proxies tracking each other in free space. (b) Object collision detection. (c) Impedance generation at object boundary. (d) Shifting of virtual proxy for tracing object outline.

penetrates the virtual object. The apparent impedance can be varied according to the type of object being displayed. For simple and sufficiently large objects employing a large stiffness, the clamp position of the virtual proxy can be set by simply minimizing the distance separating the two proxies. This allows the operator to effectively trace the outline of any given object.

In practice the position of the virtual proxy results in the continuous drift of the interface in free space as the controller attempts to match the HIP with the IHIP. This paper proposes a solution to this problem by discretizing the workspace area into a fine mesh with small grid spacing to which the IHIP is constrained. Since a force is required to displace the HIP from the IHIP, as long as the displacement between the two is not larger than the grid spacing, the interface will not drift on its own. The drawback of this method is that the user may feel a resisting force when attempting to transfer the IHIP from one cell boundary to the other in free space. The size of the cells has to be small enough such that the transition from one cell to the next is not perceived by the operator, but large enough to prevent drift of the haptic interface. This technique was successfully implemented on both haptic devices.

The impedance parameters in free space have to be fine-tuned such that stability is obtained with minimum evident damping. If the natural damping of the haptic device is sufficiently small for simulating a free space with suitable apparent permeability as a result of appropriate interface design, it is suggested that the linearizing term in (3) $\mathbf{B}\dot{\mathbf{q}}$ is omitted so that the apparent damping in free space is equivalent to the natural damping. If high object stiffness is necessary then it may be required to increase further the apparent damping to maintain stability.

5. EXPERIMENTAL SETUP

Two haptic prototypes were developed in this work: a 1-DOF joystick controller and a 4-bar parallel link manipulator. The 1-DOF joystick hand controller consists of an ergonomic hand-grip mounted on a 1cm diameter aluminum tube with a 0.2cm wall thickness 15cm in length. It incorporates two FS series force sensors available from Honeywell mounted inside the joystick handle. The stick is mounted on the shaft of the motor which provides the required actuation.

The geometry of the 4-bar parallel link manipulator, similar to the one used by Carignan and Clear [2000], is shown in Fig. 3. It consists of two pairs of 15cm aluminum tubes mounted on the sides, and two 2.5cm x 0.6cm aluminum bars 15cm length mounted on top and at the bottom. The top bar is extended by 5cm to allow for the attachment of an end effector and the mounting of force sensors. The resulting geometry is that of a parallelogram having sides of equal length l_l and an extended upper link of length l_e. The four vertices of the parallelogram are revolute joints. Link 1 is rotated through angle q_1 at the bottom joint by motor 1. Link 2 is *independently* rotated by angle q_2, also at the bottom joint, by motor 2. With this geometry, the position vector $\mathbf{p}$ of the end-effector measured with respect to the (x_1, x_2) Cartesian reference frame shown in Fig. 3 is given by

$$\mathbf{p} = \begin{pmatrix} l_l \cos q_1 - l_e \cos q_2 \\ l_l \sin q_1 - l_e \sin q_2 \end{pmatrix} \tag{14}$$

Hence the Jacobian is

$$\mathbf{J} = \begin{pmatrix} \frac{\partial \mathbf{p}}{\partial q_1} & \frac{\partial \mathbf{p}}{\partial q_2} \end{pmatrix} = \begin{pmatrix} -l_l \sin q_1 & l_e \sin q_2 \\ l_l \cos q_1 & -l_e \cos q_2 \end{pmatrix} \tag{15}$$

The dynamic equations of both haptic devices can be derived using conventional dynamic analysis techniques. For the parallel link manipulator, appropriate selection of the masses and lengths of the links led to a great simplification of the dynamic equations through cancellation of the Coriolis and centrifugal torque terms (Spong et al. [2005], Sciavicco and Siciliano [2000]).

The actuators selected for both haptic devices are 24V, 150W RE40 permanent magnet DC motors fitted with reduction gearheads from *maxon motor* capable of delivering continuous torques of 3Nm after the gearbox reduction of 12:1. The haptic devices are thus capable of comfortably displaying forces in line with the commercial PHANTOM system (Massie and Salisbury [1994]) and other similar experimental setups. The gearbox introduced an inevitable average backlash of 0.8 degrees which however did not reduce the quality of the haptic experience. Rotary incremental shaft encoders are mounted on the motor shafts to provide position sensing. Both prototypes are interfaced with a dSPACE DS1104 control board.

6. EXPERIMENTAL RESULTS

In this section, experimental results obtained using the laboratory test rigs are presented.

6.1 Impedance Generation

The results shown here concentrate on demonstrating the impedance display using the haptic controllers described in Section 3. Being the simplest, the second variant of Controller 2 on the 1-DOF joystick is discussed first. Fig. 4 depicts an experimental result of a trajectory followed by the device when a step disturbance input is applied to the current controller, effectively emulating an external torque of 1Nm. This demonstrates the haptic response to a unit

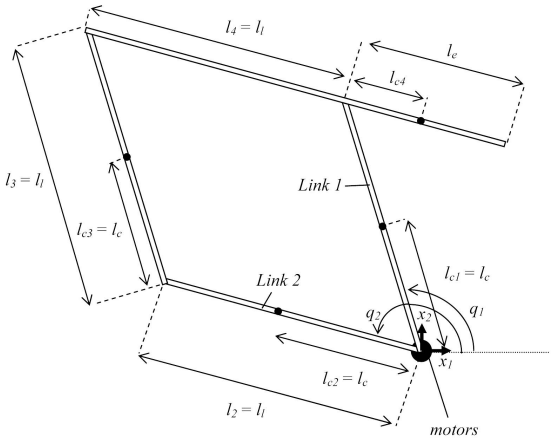

Fig. 3. Geometry of planar robotic arm.

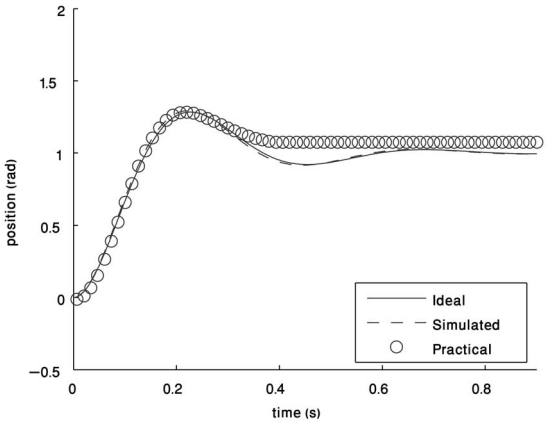

Fig. 4. Trajectory followed by single DOF interface with Controller 2 for $K_d = 1$Nm/rad and $B_d = 0.01$

step input torque generated by an operator exerting zero passive impedance. In these tests, the desired mass coefficient $\mathbf{M_d}$ is set to be equal to the inverse of the mobility tensor, $\mathbf{W^{-1}}$, of the haptic device, which reduces to the natural inertia of the device in the single DOF interface. The inaccuracy at low angular displacements from steady-state is attributed to the presence of inevitable mechanical non-linearities such as static friction which are not catered for by the model-based inverse dynamics controller utilized in this work.

The first variant of Controller 2, which achieves (6) via the use of (10), requires the use of an accurate acceleration term. However, the acceleration term estimated from the readings of the position encoders is subject to quantization effects (Colgate and Brown [1994]). Hence this approach is not favored when compared to active force feedback techniques such as Controller 1. Fig. 5 shows the behaviour of the haptic interface in response to a step unit torque for varied values of $\mathbf{M_d}$ using the acceleration term in Controller 2. The trend of increasing $\mathbf{M_d}$ is evident and compares well with the simulation results.

Controller 1 is discussed next. As shown in Section 3.1, force sensing allows for simpler control laws. It also provides a cleaner signal with which to manipulate the trajectory second order term when compared to the acceleration term obtained through differentiation of encoder position signals. Impedance display with force feedback was tested on the 1-DOF interface by physically providing stimuli to the force sensors through the application of an external load of known magnitude. The results, shown in Fig. 6, follow the expected qualitative trend. As proof of concept of Controller 1 on the parallel link manipulator, a conventional uni-directional force sensor was mounted at the tip of the end-effector and the force control algorithm was only employed in one dimension in Cartesian space. A typical behaviour of that shown in Fig. 6 was observed.

The effect of increased apparent inertia could be clearly felt along one axis in the plane of the parallel links as the sensor was pushed against. It was shown that the displayed $\mathbf{M_d}$ cannot be increased or decreased excessively: whereas large values tend to cause vibrations as the device excessively attempts to decelerate a push, low values cause the interface to accelerate excessively upon receiving an

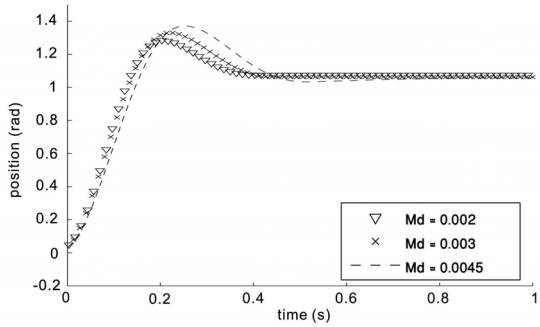

Fig. 5. Response to a unit step input torque for different desired inertias with Controller 2. $B_d = 0.05$Nms/rad and $K_d = 1$Nm/rad in each case.

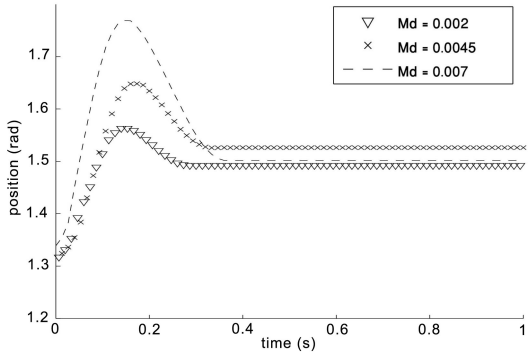

Fig. 6. Response to a unit step input torque for different desired inertias with Controller 1. $B_d = 0.03$Nms/rad and $K_d = 4$Nm/rad in each case.

input force and lose contact with the operator's finger temporarily before re-establishing contact. In practice six-axis force-torque sensors are used in n-DOF haptic devices.

Controller 3 was thoroughly tested on the parallel link manipulator - where the issue of Jacobian singularity and derivatives is relevant. It was noted that Controller 3 proved to have a performance very similar to the second variant of Controller 2 (with a typical behaviour very similar to that shown in Fig. 4) with the additional advantage that stability was ensured near the workspace boundaries where the Jacobian becomes singular. The device also remained stable while displaying impedances which were rendering Controller 2 unstable. Simulation showed that the Jacobian derivative was the most likely cause of this instability in Controller 2.

6.2 Virtual Object Display

The results shown here demonstrate the effect of object kinesthetic constraint as described in Section 4 and are obtained from experiments utilizing the 2-DOF robotic manipulator implementing the newly designed Controller 3. Haptic rendering was carried out by defining 2-D primitives (such as a circle) in Cartesian space as a desired reference contour $f(x_{d1})$ along which the virtual proxy relocates upon penetrating the object. On collision, the minimum of the function relating the distance between the virtual and manual proxy given by

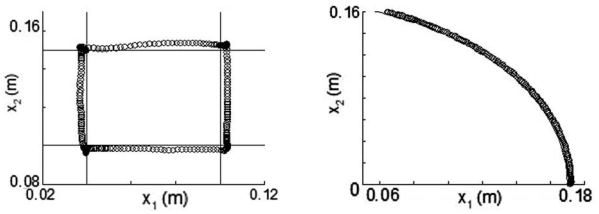

(a) (b)

Fig. 7. Tracing a virtual shape with Controller 3. (a) Square from the inside. (b) Circle from the inside. Solid line - constraint. Marked line - experimental trajectory traced by the manipulator tip.

$$d = ((x_{d1} - x_1)^2 + (f(x_{d1}) - x_2)^2)^{1/2} \tag{16}$$

was found in real-time to set a value for the virtual proxy or the desired impedance reference position.

Fig. 7 shows a sample of objects which were defined and effectively traced using the haptic interface. The stiffness $\mathbf{K_d}$ was set to 1500N/m to give the impression of a solid object. This value compares well with the 2000N/m deemed necessary to simulate an immovable wall (Massie and Salisbury [1994]). The value of $\mathbf{K_d}$ cannot be increased too much as this would result in what is known as contact instability. The damping value $\mathbf{B_d}$ was set to 5Ns/m which, in addition to that contributed by the haptic interface generated quite an effective permeability of free space and ensured stability. Since Controller 3 was utilized, the device's apparent mass was kept unchanged. The 2-D mesh in free space was created with a grid spacing of 0.3mm, which for the given stiffnesses could not be perceived by the operator.

Although this approach is notorious for some penetration inside the virtual object, this weakness is generally dismissed because humans are incapable of accurate position sensing. Springer and Ferrier [1999] state that traditional haptic devices do provide a force at the virtual wall which is proportional to the penetration distance and velocity, and propose a way to remove this penetration by introducing a decoupled actuator and *pre-contact distance sensing* thereby improving performance and stability. The God-object algorithm (Zilles and Salisbury [1995]) is a more sophisticated force-reflection method based on the above simple approach. The same principles are also used in the haptic rendering of 3D objects which involve polygons (surface rendering) or voxels (volume rendering).

7. CONCLUSIONS

This paper presents the complete design, implementation and experimental evaluation of two haptic systems. It contributes by deriving and implementing a controller resistant to Jacobian singularity and quantization effects. Moreover, all the control algorithms shown are very promising for use in commercial haptic products. The experiment results reveal the accuracy and effectiveness of the constructed haptic devices and their control, despite the extent of system modeling required. The devices are able to realistically display impedances and effective kinesthetic constraints of objects described by simple functions.

REFERENCES

R. J. Adams. Stable haptic interaction with virtual environments, 1999. URL `http://brl.ee.washington.edu/Research_Active/Haptics/Device_04_LHD/LHD.html`.

A. Albu-Schäffer and G. Hirzinger. Cartesian Impedance Control Techniques for Torque Controlled Light-Weight Robots. *Proc. of the 2002 IEEE International Conference on Robotics and Automation*, 1:657–663, May 2002.

L. Birglen, C. Gosselin, N. Pouliot, B. Monsarrat, and T. Laliberte. SHaDe, a new 3-DOF haptic device. *IEEE Transactions on Robotics and Automation*, 18:166–175, April 2002.

C. R. Carignan and K. R. Clear. Closed-Loop Force Control for Haptic Simulation of Virtual Environments. *Haptics-e: The Electronics Journal of Haptics Research. Available online at http://www.haptics-e.org*, 1(2):1–14, February 2000.

J. E. Colgate and J. M. Brown. Factors Affecting the Z-Width of a Haptic Display. *Proc. of the IEEE 1994 International Conference on Robotics & Automation*, 4: 3205–3210, May 1994.

V. Hayward, O. R. Astley, M. Cruz-Hernandez, D. Grant, and G. Robles-De-La-Torre. Haptic interfaces and devices. *Sensor Review*, 24:16–29, 2004.

N. Hogan. Impedance control - An approach to manipulation. Part I-III. *ASME Journal of Dynamic Systems and Measurement Control*, 107:1–24, March 1985.

R. Q. van der Linde, P. Lammertse, E. Frederiksen, and B. Ruiter. The HapticMaster, a new high-performance haptic interface. *Proc. Eurohaptics*, pages 1–5, July 2002.

T. H. Massie and J. K. Salisbury. The PHANToM Haptic Interface: A Device for Probing Virtual Objects. *Proc. of the ASME Winter Annual Meeting, Symposium on Haptic Interfaces for Virtual Environment and Teleoperator Systems*, 1:295–300, November 1994.

T. H. Massie and K. Salisbury Jr. US Patent 6,405,158 B1: Force Reflecting Haptic Interface, June 2002.

M. L. McLaughlin, J. P. Hespanha, and G. S. Sukhatme, editors. *Touch in Virtual Environments*. Prentice-Hall, 2002.

L. Sciavicco and B. Siciliano. *Modelling and Control of Robot Manipulators*. Springer, 2000.

M. W. Spong, S. Hutchinson, and M. Vidyasagar. *Robot Modeling and Control*. Wiley, 2005.

S. L. Springer and N. J. Ferrier. A New Method for Design and Control of Haptic Interfaces for Display of Rigid Surfaces. In *ASME International Congress and Exposition, Nashville, TN, USA*, 1999.

R. J. Stone. Haptic Feedback: A Potted History, From Telepresence to Virtual Reality. *Proc. of the International Workshop on Haptic Human-Computer Interaction*, pages 1–8, August 2000.

R. A. Volpe. *Real and Artificial Forces in the Control of Manipulators: Theory and Experiments*. PhD thesis, Carnegie Mellon University, Pittsburgh, PA 15213, 1990.

C. B. Zilles and J. K. Salisbury. A Constraint-based God-object Method For Haptic Display. *Proc. of the IEEE/RSJ International Conference on Intelligent Robots and Systems, Human Robot Interaction, and Cooperative Robots*, 3:146–151, August 1995.